

Oxidation Behavior of CO Catalyzed by Several Decahedral Au Clusters: Role of Cluster Stability and Electric Field

W. Liu, Y. F. Zhu,[†] and Q. Jiang*

Key Laboratory of Automobile Materials, Ministry of Education, and School of Materials Science and Engineering, Jilin University, Changchun 130022, China

Received: August 2, 2010; Revised Manuscript Received: October 15, 2010

First-principles calculations are performed to study the adsorption and oxidation of CO on three decahedral Au clusters with the stability sequence of $\text{Au}_{146} > \text{Au}_{75} > \text{Au}_{101}$. Our calculations suggest that a cluster with a moderate stability should be an ideal catalyst when structural differences are excluded. As exemplified in our case, Au_{75} is the best catalyst since O_2 adsorption on Au_{146} is endothermic (adsorption energy $E_{\text{ad}} = -0.13$ eV), whereas CO oxidation on Au_{101} has the highest activation energy ($E_{\text{a}} = 0.75$ eV). Reactions are found to be particularly sensitive to the direction and intensity of an electric field, where the magnitude of E_{a} is considerably lowered from 0.55 to 0.32 eV after superimposing a -0.005 au field into the Au_{75} cluster. The promoted reactivity in the oxidation stage is ascribed to the lowered Fermi level and enhanced charge transfer between the adsorbates and the catalyst. Our calculations demonstrate that moderate field intensity is a better option for CO oxidation reaction since a strong electric field dramatically weakens the adsorption of the reactants.

1. Introduction

Gold nanoclusters have been extensively studied from both the experimental and theoretical points of view,^{1–5} due to their unique structures and interesting applications in catalysis,^{6–10} nanodevices,^{11,12} and life science.^{13,14} Geometry and symmetry vary as particle sizes decrease where evident size effects are observed partly due to the increase of the surface/volume ratio.^{15–17} In the case of Au clusters, icosahedrons, decahedrons, and octahedrons are energetically the lowest structures in the small, medium, and large size ranges.¹⁵ Despite the fact that bulk Au is extremely inert in chemistry, extraordinary catalytic activities of Au clusters have been demonstrated in the reactions of CO oxidation,^{17–23} propylene hydrogenation,²⁴ O_2 dissociation,²⁵ and selective oxidation of styrene,^{26,27} among which low-temperature CO oxidation has been most widely studied.

Experimentally, new synthesis techniques have made it possible to precisely control the size and shape of Au clusters.²⁸ Numerous approaches have been applied to the study of Au clusters, ranging from transmission electron microscopy (TEM), reflection absorption infrared spectroscopy (RAIRS), temperature programmed desorption (TPD), X-ray photoelectron spectroscopy (XPS), etc.^{6,16,26,29,30} Available experimental data regarding the geometric structure, vibrational spectrum, oxidation efficiency, and electronic property have been compiled from current literature. Even with this level of understanding, a definitive description of the bonding interactions, reaction mechanism, and charge distribution solely from experiments, especially in a size range of 1–3 nm, has yet to be elucidated.³¹

Theoretically, first-principles density functional theory (DFT) has evolved as an essential tool in the study of catalytic reactions, which can offer detailed information at atomic and electronic levels, and help to analyze the underlying physics.^{31–33} The total rate of reaction is limited by both adsorption and

oxidation rates,²⁰ which can be described by the magnitudes of adsorption energy E_{ad} and activation energy E_{a} , respectively. A review of recent literature shows that the reactivity of Au clusters is strongly dependent on the oxide support,^{18,34–36} metal alloying,^{17,20,37} moisture content,^{36,38,39} and particle size.^{7,10,17,40} Nevertheless, STM, TPD, and RAIRS revealed that the exceptional reactivity of Au clusters was in fact attributed to the highly uncoordinated atoms, not the quantum size effects.⁶ This conclusion was attained based on the fact that thin islands of Au have the same CO adsorption behavior as large Au particles and extended Au surfaces.⁶

An interesting question is naturally posed, i.e., which factor will dominate the reactions when various catalysts have the same uncoordinated atoms (or shape effects)? To clarify this question, three decahedral Au clusters are chosen as prototype materials in the present work.^{41–43} All clusters have the same minimum Marks-decahedral (m-Dh) motif, with increasing magic number of 75, 101, and 146 (shown as Au_{75} , Au_{101} , and Au_{146}). Examination of the energies showed that their stabilities have a sequence of $\text{Au}_{146} > \text{Au}_{75} > \text{Au}_{101}$, which implies that Au_{75} corresponds to the moderate stable structure.^{15,29} Although many works were centered on CO oxidation on Au, a systematic study of CO oxidation for a series of *lowest-energy Au clusters with the same motif* is still lacking, which should benefit for actual applications and the pure stability effect where the structure difference is excluded. Moreover, via superimposing an external electric field, the reaction process is expected to be altered due to the charge redistribution within the system. Thus, field strength F could be an alternate tool to effectively distinguish the catalytic capacity. In this study, we aim to examine how the cluster stability influences catalytic behaviors when the shape effect is excluded, and also investigate the underlying relationship between Fermi level and catalytic reactivity that is induced by electric fields.

In this contribution, Au_{75} , Au_{101} , and Au_{146} clusters with the same m-Dh motif are taken as catalysts for CO oxidation. The nudged elastic band (NEB) method is employed to determine

*To whom correspondence should be addressed. E-mail: jiangq@jlu.edu.cn.

[†] Fax: +86 431 85095876. E-mail: yfzhu@jlu.edu.cn.

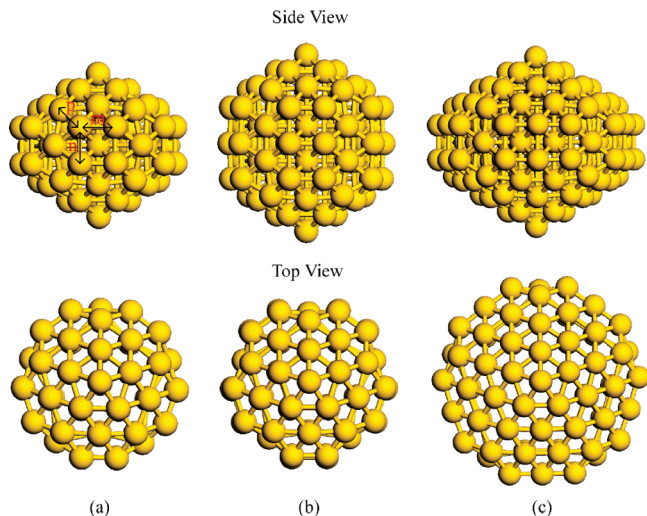


Figure 1. Schematic plots for the decahedral Au clusters with $N = 75$ (a), 101 (b), and 146 (c).

the minimum-energy pathway (MEP). Electric fields with different directions and intensities are superimposed into the Au₇₅ cluster. Our results validate that the cluster stability and Fermi level dominate the catalytic reactivity.

2. Computational Framework

The spin-unrestricted DFT calculations are performed with the DMol³ code.^{44,45} Generalized gradient approximation (GGA) with Perdew and Wang (PW91)⁴⁶ is invoked as the exchange-correlation functional. The DFT Semicore Pseudopotentials (DSPP) core treat method is implemented for relativistic effects, and the double numerical atomic orbital augmented by a polarization function (DNP) is employed as the basis set. A 0.002 Ha of smearing to the orbital occupation and 5.5 Å of global orbital cutoff radius are applied to achieve accurate electronic convergence. The minimization of the reaction pathways and the search of the transition state (TS) are performed with the NEB method.⁴⁷ The “Electric_Field” keyword in the DMol³ code allows us to specify the direction and intensity of an electric field.

All decahedral Au clusters involved in this work are depicted in Figure 1. In terms of (m,n,p) naming nomenclature, particles with the number of atoms $N = 75$, 101, and 146 can be named as (2,2,2), (2,3,2), and (3,2,2) decahedrons, respectively.⁴⁸ In addition to sharing the one edge coinciding with the 5-fold axis, the subunits of a decahedron are joined to adjacent tetrahedral by twin boundaries.² The Au(111) surface with a (2×2) unit cell and seven layers is also established for a comparison purpose. The k -point is set to $5 \times 5 \times 1$ and a vacuum width of 12 Å is used for the surface, which ensures the interaction between repeated slabs in direction normal to the surface being small enough. All atoms are allowed to relax in the cluster models, whereas in the slabs only the two uppermost layers are allowed to fully relax.

The surface energy γ values of 55 metallic elements have been successfully predicted by $\gamma = -[2 - Z_s(\infty)/Z_B - [Z_s(\infty)/Z_B]^{1/2}]E_c/2$ in one of our theoretical works,⁴⁹ where E_c denotes the cohesive energy, $Z_s(\infty)$ denotes the coordination numbers (CN) of bulk surface atoms, and Z_B denotes the CN within the crystals. Here, the above equation is extended to clusters in the nanometer scale range, and thus the size-dependent surface energy $\gamma(N)$ can be determined as:

$$\gamma(N) = [2 - Z_s(N)/Z_B - [Z_s(N)/Z_B]^{1/2}]E_c(N)/2 \quad (1)$$

where $Z_s(N)$ and $E_c(N)$ indicate the average CN of surface atoms and the average E_c value within a cluster, respectively. Note that $Z_s = N_b/N_s$, where N_s denotes the number of surface atoms and N_b is the number of their bonds in total. All $E_c(N)$ values are obtained from the same GGA-PW91 functional to ensure data consistency.

Different sites were considered for CO adsorption, and our results show that the uppermost (or bottommost) vertex is energetically most favorable in Au clusters. Moreover, prior experiments and simulations reported indicate that CO prefers to stay at the atop site of the Au(111) surface.^{50,51} Thus, CO in our simulation is placed at the uppermost vertex in the cluster models and at the atop site in the slab. The initial C–O distance is set to be 1.13 Å in light of available experimental data.⁵² The adsorption energy of CO, E_{adCO} , is the difference between the total energy of the considered system, $E_{(CO+Au)}$, and that of the corresponding cluster (E_{Au}) and free gas (E_{CO}), namely:

$$E_{adCO} = E_{(CO+Au)} - E_{Au} - E_{CO} \quad (2)$$

The initial state (IS) of the reaction is created by bonding an O₂ molecule to the above CO preadsorbed system. In this case, the coadsorption energy of CO + O₂, E_{adIS} , can be measured as:

$$E_{adIS} = E_{(CO+Au+O_2)} - E_{Au} - E_{CO} - E_{O_2} \quad (3)$$

where the subscripts “CO+Au+O₂” and “O₂” denote the coadsorption system and the free O₂ molecule, respectively.

Moreover, the binding energy of O₂ on the CO preadsorbed system, E_{adO_2} , can be determined by:

$$E_{adO_2} = E_{(CO+Au+O_2)} - E_{(CO+Au)} - E_{O_2} \quad (4)$$

In terms of the above equations, eq 4 can be readily obtained by subtracting eq 2 from eq 3, i.e., $E_{adO_2} = E_{adIS} - E_{adCO}$.¹⁷

Oxidation of the first CO is solely considered in this work since it has been proven to be the rate-limiting step in an oxidation reaction.²² The full reaction pathways involving all the stages of adsorption, oxidation, and desorption are considered for a comprehensive study. In the oxidation stage, the magnitudes of E_a and reaction energy E_r are defined as the energy of the transition state (TS) and the metastable state (MS) minus that of the IS, respectively. In the desorption stage, E_a' is defined as the energy of the TS' minus that of the MS, while E_r' is defined as the energy of the final state (FS) minus that of the MS. Consequently, MS plays an essential role in the entire reaction, which acts as the product in the oxidation stage and the reactant in the desorption stage.

3. Results and Discussion

The calculated $E_c(N)$ and $\gamma(N)$ values of the bare Au clusters and (111) surface are shown in Table 1. The magnitudes of $E_c(N)$ are -2.48 , -2.53 , -2.60 , and -2.92 eV/atom, when $N = 75$, 101, 146, and ∞ , respectively. Thus, $E_c(N)$ is a function of the surface bond deficit and decreases monotonically as N increases. In light of eq 1, $\gamma(N)$ of the m-Dh structure, in a reverse order of $E_c(N)$, slightly decreases as N increases. The values of Au clusters are almost identical since both energy

TABLE 1: Computed E_c , γ , E_{ad} , E_a , E_r , E'_a , and E'_r (in eV) for Three Decahedral Au Clusters with $N = 75$, 101, and 146^a

Au	N	$-E_c$	N_s	N_b	Z_s	γ
clusters	75	2.48	57	422	7.40	0.74
	101	2.53	72	542	7.53	0.73
	146	2.60	97	752	7.75	0.72
(111) surface	∞	2.92			9.00	0.56

Au	N	adsorption			oxidation		desorption	
		$-E_{adCO}$	$-E_{adIS}$	$-E_{adO_2}$	E_a	$-E_r$	E'_a	$-E'_r$
clusters	75	0.81	0.89	0.08	0.55	0.48	0.23	2.26
	101	0.75	1.03	0.28	0.75	0.36	0.29	2.35
	146	0.78	0.65	-0.13	0.33	0.56	0.41	2.10
(111) surface	∞	0.13	-0.28	-0.41				

^a The data for the Au(111) surface are also listed for comparison. For the definitions of the related amounts with other symbols see the text.

values of the surface atoms and inner atoms increase simultaneously as N decreases.⁵³ Nevertheless, the γ values of clusters (0.72–0.74 eV) are much larger than that of the Au(111) surface (0.56 eV), which confirms the extraordinary activity of Au clusters.

The CO adsorption data are also listed in Table 1, from which $-E_{adCO}(N) = 0.81, 0.75$, and 0.78 eV for Au₇₅, Au₁₀₁, and Au₁₄₆, respectively. For comparison, the adsorption results of Au(111) surface are also listed in the table. Differing from small clusters, the interaction between CO and Au(111) is very weak, where $E_{adCO}(\infty) = -0.13$ eV from the present work and -0.17 eV from literature data.⁷ We have also considered the coadsorption of CO + O₂ on the Au(111) surface, where the positive binding energy (+0.28 eV) implies that there is no stable molecular state on this flat surface. Moreover, binding of O₂ at the CO preadsorbed Au(111) surface is also very endothermic (+0.41 eV). Blyholder's model states that one lone pair of electrons are donated from the nonbonding CO-5 σ orbital into empty metal orbitals, and back-donated from occupied metal d orbitals to the empty CO-2 π^* orbital, simultaneously.⁵⁴ Thus, the variation of binding can be determined by the coupling of 2 π^* -d and estimated based on the bond length of C–Au, d_{C-Au} . In our case, the d_{C-Au} values are 1.981, 1.992, and 1.990 Å when CO is adsorbed on Au₇₅, Au₁₀₁, and Au₁₄₆, respectively, which coincides with the sequence of our calculated $E_{adCO}(N)$.

The above CO adsorption behaviors can be further interpreted in terms of the plots of partial density of states (PDOS). As shown in Figure 2, the bands of adsorbed CO (plot c) and Au₇₅ (plot d) move left to the lower energy range in comparison to those of the free CO molecule (plot a) and bulk Au crystal (plot b). Both CO-5 σ and CO-1 π orbitals broaden and dominate the interaction, where 5 σ orbital shifts below the 1 π orbital. CO-4 σ orbital is localized below -10 eV after adsorption and hybridizes with a new peak of Au composed of d+s+p at the lowest energy range. All peaks of CO overlap accurately with those of the Au atom, and thus the chemical bond between CO and Au is present. Similar electronic structures can also be seen in the CO/Au₁₀₁ and CO/Au₁₄₆ systems as depicted in plots e–h. The height of the peaks at the Fermi level shows that the Au crystal in plot b has the smallest magnitude of 0.38, whereas the Au₇₅ in plot d has the largest value of 0.93. This result suggests that the activity of a substrate can be roughly judged by the intensity at the Fermi level.

Using the E_{adCO} value as a starting point, the minimum reaction paths for each cluster are illustrated in Figure 3, where the left, middle, and right parts indicate the adsorption, oxidation,

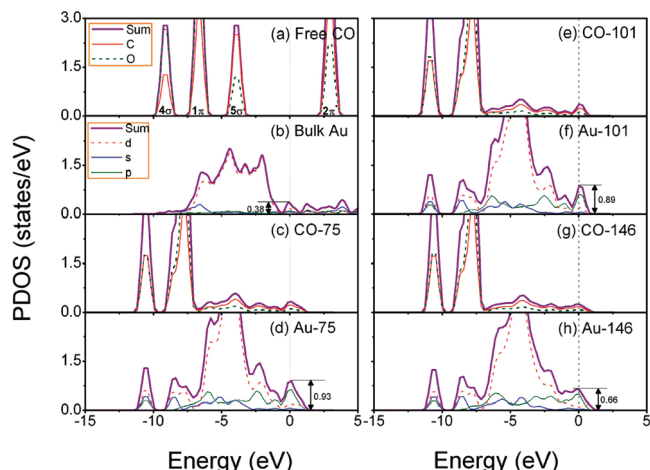


Figure 2. Size-dependent PDOS plots for CO on Au clusters. For comparison, plots of free CO gas and the bulk Au crystal are also plotted. The Fermi level is set to be zero and indicated by a dashed line.

and desorption stages, respectively. In the first step, it is readily seen that CO is strongly bonded on all three clusters, where Au₇₅ has the smallest while Au₁₀₁ has the largest E_{adCO} value. Subsequently, molecular O₂ is coadsorbed on the Au₂ and Au₃ atoms in the second layer (the atoms are labeled in Figure 3a), with CO preadsorbed on the Au₁ atom in the uppermost vertex. The relaxed IS structures show that CO remains vertical to the clusters, while the O₂–O₃ bond is parallel to the neighboring Au–Au bond, which is consistent with the conditions of CO oxidation on Au₅₅, Ag₅₅, and Au₂₅Ag₃₀ clusters.²⁰ In this case, the bonding strength between CO + O₂ and Au₁₀₁ is the strongest with $E_{adIS} = -1.03$ eV. If this value is chosen as a reference, $E_{adIS} = -0.65$ eV for Au₁₄₆ is 36.89% higher. It is worth pointing out that the step of O₂ adsorption is endothermic in the case of Au₁₄₆, as shown in Figure 3c and Table 1, although the energy difference is small ($E_{adO_2} = +0.13$ eV). Consequently, coadsorption of O₂ on the CO preadsorbed Au₁₄₆ cluster hardly happens spontaneously, which is apparently detrimental to the entire reaction rate.

In the oxidation stage, Au₁₀₁, Au₇₅, and Au₁₄₆ have the largest ($E_a = 0.75$ eV), moderate (0.55 eV), and lowest (0.33 eV) reaction barriers, respectively. Noteworthy is the fact that the reaction rate has an exponential relationship with the reaction barrier,⁵⁷ and the catalytic reactivity of Au₁₀₁ thus should be dramatically worse than that of Au₇₅. This result is confirmed by the corresponding $E_r(N)$ values shown in Table 1 and Figure 3, from which Au₁₀₁ has the lowest reaction driving force with $E_r = -0.36$ eV. Comparing the E_a and E_{adIS} values listed in Table 1 reveals that the oxidation rate is proportional to the binding energy between the reactants and catalysts. This is because stronger adsorbing reactants tend to retard bond formation steps, due to the deep energy sink development on the potential energy surfaces of the respective oxidation processes.⁵⁵ Thus, looser bonding could benefit for catalyzing CO oxidation. The final step is desorption of the nascent CO₂, and in this case the MS in Figure 3 becomes the reactant. The bond between O₂ and O₃ continuously elongates and then breaks. The fragment of O₁–C–O₂ continually moves away from the substrate and finally produces a free CO₂ gas. The third bond is formed between O₃ and its neighboring Au atom, and the former located stably at the hollow site in FS. Our calculation shows that Au₇₅ has the lowest desorption activation energy (0.23 eV) whereas Au₁₄₆ has the largest one (0.41 eV). According to the above discussion, Au₇₅ performs the best in

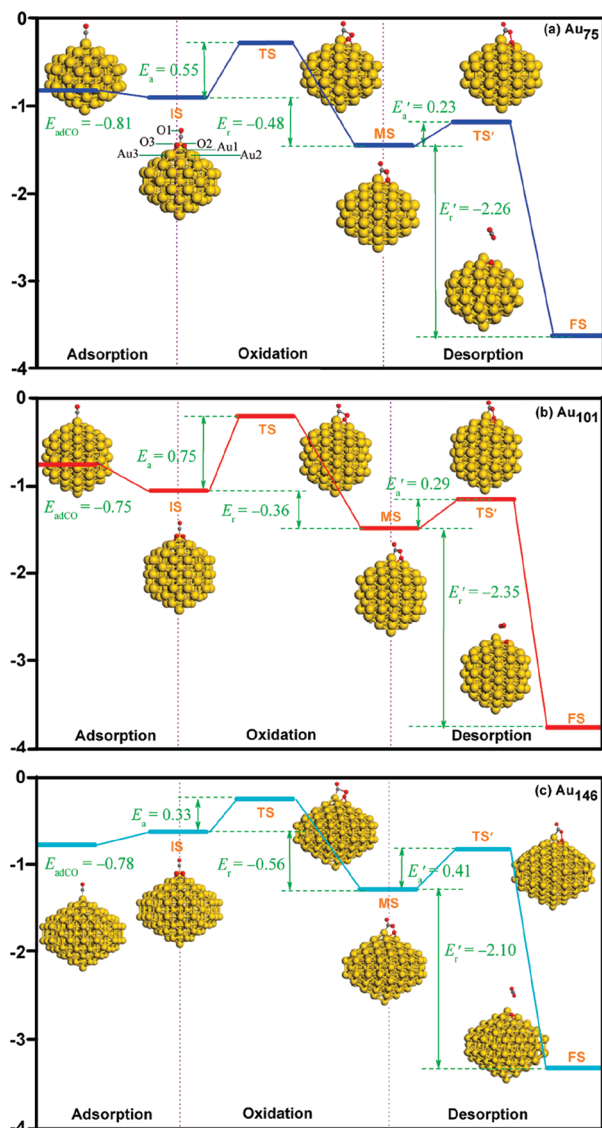


Figure 3. Snapshots of the minimum energy path (MEP) for CO adsorption (left), oxidation (middle), and desorption (right) on Au clusters. The yellow, gray, and red spheres represent Au, C, and O atoms, respectively.

this catalytic reaction due to the weakest adsorption capacity and the largest E'_a of Au₁₄₆, as well as the largest E_a of Au₁₀₁ among them. Given that the cluster stability has a sequence of Au₁₄₆ > Au₇₅ > Au₁₀₁,^{15,29} our calculations reveal that a cluster with a moderate stability should be an ideal catalyst when the shape effect is excluded.

The geometric parameters of the oxidation stage are measured and listed in Table 2, where the subscripts "O1", "O2", and "O3" indicate the O atom in CO, and in the original free O₂ molecule, respectively. As exemplified in Au₇₅, the magnitudes of d_{O1-C} and d_{C-Au1} increase continuously in the entire oxidation process since the newly formed O2-C bond weakens the interactions of O1-C and C-Au1. The gradual movement of O2 from Au2 renders the increase of the d_{O2-Au2} value. d_{O2-O3} decreases from 1.341 Å in IS to 1.310 Å in TS, and then increases to 1.468 Å in MS, which is attributed to the formation of the O2-C bond. d_{O2-C} decreases considerably from 3.176 to 1.369 Å, which confirms the formation of the nascent CO₂ molecule. The angle of the O1-C-O2 fragment α increases from 107.591° in IS to 118.603° in MS. Similar geometric variation trends are also found in the Au₁₀₁ and Au₁₄₆ systems.

TABLE 2: Geometric Parameters (Bond Length d in Å and Bond Angle α of the O1-C-O2 Fragment in deg) for CO Oxidation on the Au Clusters with $N = 75, 101$, and 146

	parameter ^a	IS	TS	MS
Au-Dh-75	d_{O1-C}	1.144	1.156	1.206
	d_{C-Au1}	1.999	2.051	2.088
	d_{O2-Au2}	2.196	2.723	3.273
	d_{O2-O3}	1.341	1.310	1.468
	d_{O2-C}	3.176	2.055	1.369
	α	107.591	117.874	118.603
Au-Dh-101	d_{O1-C}	1.144	1.145	1.207
	d_{C-Au1}	1.989	2.043	2.093
	d_{O2-Au2}	2.205	2.747	3.299
	d_{O2-O3}	1.342	1.380	1.468
	d_{O2-C}	3.265	2.125	1.371
	α	109.754	118.304	118.358
Au-Dh-146	d_{O1-C}	1.146	1.140	1.208
	d_{C-Au1}	2.002	2.052	2.093
	d_{O2-Au2}	2.473	2.905	2.343
	d_{O2-O3}	1.286	1.339	1.465
	d_{O2-C}	3.343	2.158	1.363
	α	108.708	118.501	119.451

^a O1, O2, and O3 indicate the original O atom in CO, and the original free O₂ molecule, respectively. We assume that O2 reacts with CO first, and leaves the O3 atom on the Au cluster.

Some regularity can be achieved in comparison with the three clusters. For example, $d_{C-Au1} = 1.999, 1.989$, and 2.002 Å in IS for Au₇₅, Au₁₀₁, and Au₁₄₆, respectively, which confirms that CO + O₂ has the largest binding on Au₁₀₁, as well as the weakest binding on Au₁₄₆. Moreover, α in MS has the sequence of Au₁₀₁ < Au₁₄₆ < Au₇₅, which is in contrast with that of their corresponding E_a values. Hence, a larger α is related to a lower barrier in the oxidation reaction.

Our electric field calculations show that the catalytic reactivity in the CO oxidation stage can be further enhanced in the presence of a negative field. As exemplified in Au₇₅, the magnitudes of E_a and E_r drop to 0.32 and -0.78 eV, respectively, at $F = -0.005$ au. Plots a and b in Figure 4 illustrate that the E_a curve declines continuously with more negative F ranging from -0.007 to -0.012 au, where the smallest $E_a = 0.18$ eV appears at $F = -0.012$ au. In contrast, a positive field is deleterious to CO oxidation due to the increase of both the E_a and E_r values. Note that E_r becomes positive at $F > 0.009$ au, which implies that the stability of MS is even lower than that of IS, and thus this reaction hardly occurs. The Fermi energy (E_f) values are found to be strongly affected by F (see Figure 4c), from which $E_f = -5.21, -10.04, -16.70, -0.44$, and $+6.23$ eV under $F = 0.000, -0.005, -0.012, +0.005$, and $+0.012$ au, respectively. As depicted in Figure 4d, E_f moves considerably toward the lower energy range with negative fields, and more importantly, the band intensity across E_f is significantly enhanced with the increase of the intensity. In contrast, the positive field shifts the Fermi level to a higher energy range. This result suggests that the position of the Fermi level and the charge redistribution are sensitive to the electric field and have a direct relationship with the catalytic reactivity.

Charge distributions of Au₇₅ cluster in MS are studied by the Hirshfeld analysis method and the results are depicted in Figure 5. Electron flows from Au1 and Au2 to the adsorbed C and O3 atoms in the absence of a field, where the charge carried by Au1 (or Au2) increases from -0.006 to $0.062 e$ (or from -0.003 to $0.060 e$) after CO₂ is adsorbed. Au4 is located in the middle of the cluster and only carries $0.001 e$. In contrast, all Au atoms in the lower part of the cluster carry negative charges ranging from -0.007 to $-0.021 e$. At $F = +0.012$ au, the

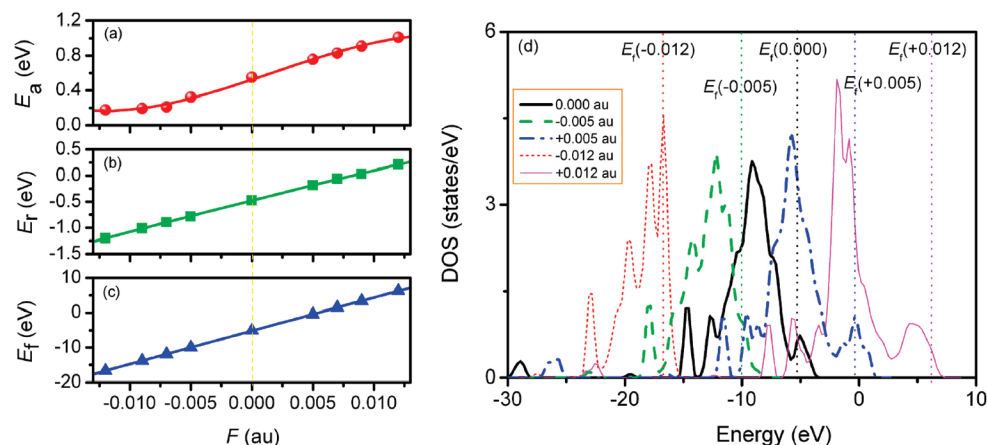


Figure 4. Field intensity-dependent E_a (a), E_r (b), and E_f (c) results for CO oxidation on the Au₇₅ cluster, where the discrete data are fitted by a third-order exponential function. DOS plots of the vertex Au1 atom in TS are shown in plot d, where the Fermi levels are labeled by dashed lines when $F = -0.012, -0.005, 0.000, +0.005$, and $+0.012$ au.

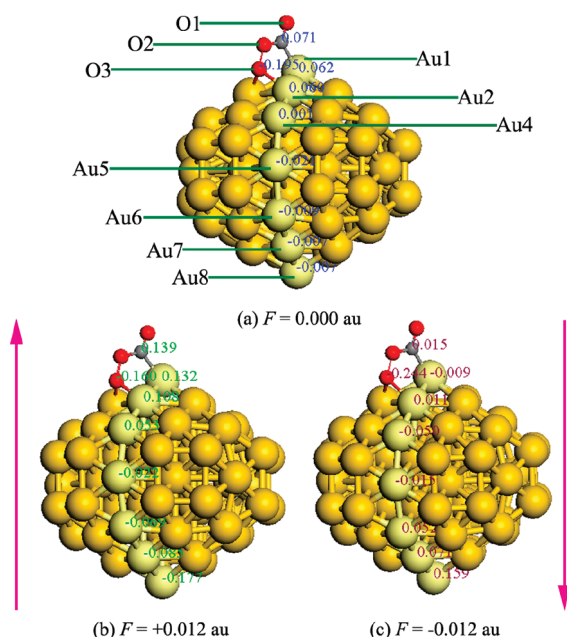


Figure 5. Hirshfeld charge analysis results for the MS state of the Au₇₅ clusters under (a) $F = 0.000$ au, (b) $F = +0.012$ au, and (c) $F = -0.012$ au. Arrows in the figure indicate the direction of the electric field that superimposed into the systems.

positive charge carried by C increases from 0.071 to 0.139 e while the negative charge carried by O3 increases from -0.195 to -0.160 e , as shown in Figure 5b. This result implies that a positive field drops the charge of the adsorbate obtained from the substrate. In comparison with plot a, the charges carried by Au1 and Au2 are nearly doubled in plot b, and that by Au4 is enhanced significantly from 0.001 to 0.053 e . However, Au atoms in the lower part of the cluster obtain charges, increasing in lower layers. The charge carried by Au5 to Au8 continuously decreases from -0.022 , -0.069 , -0.085 , and -0.177 e , respectively. Namely, charges move downward in the presence of a positive field. An opposite charge transfer direction can be achieved with a negative field. When $F = -0.012$ au shown in Figure 5c, C is less positive (0.015 e) while O3 is more negative (-0.244 e). Au1 and Au4 become anions and carry -0.009 and -0.050 e , respectively, while Au2 carries significantly less charge (0.011 e). Since charges move upward, Au6 to Au8 in the lower layers lose charges and become cations.

The full reaction pathways of Au₇₅ with and without an electric field are determined and compared to understand the

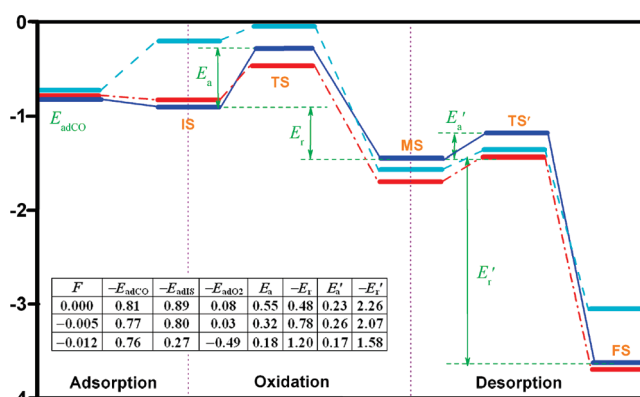


Figure 6. Snapshots of the minimum energy path (MEP) for CO adsorption (left), oxidation (middle), and desorption (right) on the Au₇₅ cluster with and without electric field. The solid, dashed-dotted, and dashed lines denote the results under 0.000, -0.005 , and -0.012 au fields, respectively.

effect of a field on the entire reaction. As shown in Figure 6, despite the adsorption of the reactants being slightly weakened from -0.89 to -0.80 eV after superimposing a -0.005 au field, the magnitude of E_a is considerably decreased from 0.55 to 0.32 eV in the oxidation stage, and E'_a remains almost the same in the desorption stage. With applying the -0.012 au field, the adsorption of CO (-0.76 eV) and coadsorption of CO + O₂ (-0.27 eV) remains exothermic. However, the binding of O₂ ($+0.49$ eV) becomes very unfavorable on the surface sites as shown in Figure 5. A quandary is thus presented since on the one hand a strong electric field, e.g., -0.012 au, can dramatically lower the oxidation reaction barrier; on the other hand, the adsorption of the reactants is deteriorated. According to the above discussion, a negative field with a moderate intensity would be a better option, which simultaneously ensures that the adsorption is exothermic and the activation energy is significantly lowered in the CO oxidation reaction.

4. Conclusions

In conclusion, DFT calculation were carried out to study the CO oxidation behaviors on three decahedral Au clusters. The Au₇₅ cluster with a moderate stability is ideal among the three catalysts since Au₁₄₆ hinders the gas adsorption, whereas Au₁₀₁ tends to retard the formation of nascent CO₂ according to our results. The sequence of the E_a values was found to be consistent with that of their corresponding CO + O₂ coadsorption energies.

Moreover, a negative field lowers the Fermi level and enhances the charge transfer, and thus decreases the reaction barrier in the CO oxidation stage.

Acknowledgment. Financial support by NNSFC (Grant No. 60876074), Program for New Century Excellent Talents in University (NCET-08-0246), National Key Basic Research Development Program (Grant No. 2010CB631001), Program for Changjiang Scholars and Innovative Research Team in University, and Young Scholar Projects in Jilin University (200905001) is acknowledged.

References and Notes

- (1) Li, Z. Y.; Young, N. P.; Di Vece, M.; Palomba, S.; Palmer, R. E.; Bleloch, A. L.; Curley, B. C.; Johnston, R. L.; Jiang, J.; Yuan, J. *Nature* **2008**, *451*, 46.
- (2) Johnson, C. L.; Snoeck, E.; Ezcurdia, M.; Rodriguez-Gonzalez, B.; Pastoriza-Santos, I.; Liz-Marzan, L. M.; Hytch, M. J. *Nat. Mater.* **2008**, *7*, 120.
- (3) Pastoriza-Santos, I.; Sanchez-Iglesias, A.; de Abajo, F. J. G.; Liz-Marzan, L. M. *Adv. Funct. Mater.* **2007**, *17*, 1443.
- (4) Jadzinsky, P. D.; Calero, G.; Ackerson, C. J.; Bushnell, D. A.; Kornberg, R. D. *Science* **2007**, *318*, 430.
- (5) Herzing, A. A.; Kiely, C. J.; Carley, A. F.; Landon, P.; Hutchings, G. J. *Science* **2008**, *321*, 1331.
- (6) Lemire, C.; Meyer, R.; Shaikhutdinov, S.; Freund, H. J. *Angew. Chem., Int. Ed.* **2004**, *43*, 118.
- (7) Liu, Z. P.; Hu, P.; Alavi, A. J. *Am. Chem. Soc.* **2002**, *124*, 14770.
- (8) Zhou, X.; Xu, W.; Liu, G.; Panda, D.; Chen, P. J. *Am. Chem. Soc.* **2010**, *132*, 138.
- (9) Matthey, D.; Wang, J. G.; Wendt, S.; Matthiesen, J.; Schaub, R.; Laegsgaard, E.; Hammer, B.; Besenbacher, F. *Science* **2007**, *315*, 1692.
- (10) Lopez-Acevedo, O.; Kacprzak, K. A.; Akola, J.; Hakkinen, H. *Nat. Chem.* **2010**, *2*, 329.
- (11) Stewart, M. E.; Anderton, C. R.; Thompson, L. B.; Maria, J.; Gray, S. K.; Rogers, J. A.; Nuzzo, R. G. *Chem. Rev.* **2008**, *108*, 494.
- (12) Anker, J. N.; Hall, W. P.; Lyandres, O.; Shah, N. C.; Zhao, J.; Van Duyne, R. P. *Nat. Mater.* **2008**, *7*, 442.
- (13) Daniel, M. C.; Astruc, D. *Chem. Rev.* **2004**, *104*, 293.
- (14) Sassolas, A.; Leca-Bouvier, B. D.; Blum, L. J. *Chem. Rev.* **2008**, *108*, 109.
- (15) Bao, K.; Goedecker, S.; Koga, K.; Lancon, F.; Neelov, A. *Phys. Rev. B* **2009**, *79*, 041405.
- (16) Gruene, P.; Rayner, D. M.; Redlich, B.; van der Meer, A. F. G.; Lyon, J. T.; Meijer, G.; Fielicke, A. *Science* **2008**, *321*, 674.
- (17) Gao, Y.; Shao, N.; Bulusu, S.; Zeng, X. C. *J. Phys. Chem. C* **2008**, *112*, 8234.
- (18) Haruta, M.; Kobayashi, T.; Sano, H.; Yamada, N. *Chem. Lett.* **1987**, 405.
- (19) Molina, L. M.; Hammer, B. *J. Catal.* **2005**, *233*, 399.
- (20) Chang, C. M.; Cheng, C.; Wei, C. M. *J. Chem. Phys.* **2008**, *128*, 124710.
- (21) Hartshorn, H.; Pursell, C. J.; Chandler, B. D. *J. Phys. Chem. C* **2009**, *113*, 10718.
- (22) Prestianni, A.; Martorana, A.; Ciofini, I.; Labat, F.; Adamo, C. *J. Phys. Chem. C* **2008**, *112*, 18061.
- (23) Guzman, J.; Gates, B. C. *J. Am. Chem. Soc.* **2004**, *126*, 2672.
- (24) Chou, J.; Franklin, N. R.; Baeck, S. H.; Jaramillo, T. F.; McFarland, E. W. *Catal. Lett.* **2004**, *95*, 107.
- (25) Lyalin, A.; Taketsugu, T. *J. Phys. Chem. Lett.* **2010**, *1*, 1752.
- (26) Turner, M.; Golovko, V. B.; Vaughan, O. P. H.; Abdulkhin, P.; Berenguer-Murcia, A.; Tikhov, M. S.; Johnson, B. F. G.; Lambert, R. M. *Nature* **2008**, *454*, 981.
- (27) Gao, W.; Chen, X. F.; Li, J. C.; Jiang, Q. *J. Phys. Chem. C* **2010**, *114*, 1148.
- (28) Sanchez-Iglesias, A.; Pastoriza-Santos, I.; Perez-Juste, J.; Rodriguez-Gonzalez, B.; de Abajo, F. J. G.; Liz-Marzan, L. M. *Adv. Mater.* **2006**, *18*, 2529.
- (29) Cleveland, C. L.; Landman, U.; Schaaff, T. G.; Shafigullin, M. N.; Stephens, P. W.; Whetten, R. L. *Phys. Rev. Lett.* **1997**, *79*, 1873.
- (30) Liu, X. Y.; Wang, A. Q.; Wang, X. D.; Mou, C. Y.; Zhang, T. *Chem. Commun.* **2008**, 3187.
- (31) Gao, Y.; Shao, N.; Zeng, X. C. *ACS Nano* **2008**, *2*, 1497.
- (32) Garzon, I. L.; Michaelian, K.; Beltran, M. R.; Posada-Amarillas, A.; Ordejon, P.; Artacho, E.; Sanchez-Portal, D.; Soler, J. M. *Phys. Rev. Lett.* **1998**, *81*, 1600.
- (33) Pei, Y.; Gao, Y.; Shao, N.; Zeng, X. C. *J. Am. Chem. Soc.* **2009**, *131*, 13619.
- (34) Amft, M.; Skorodumova, N. V. *Phys. Rev. B* **2010**, *81*, 195443.
- (35) Jiang, H. L.; Liu, B.; Akita, T.; Haruta, M.; Sakurai, H.; Xu, Q. *J. Am. Chem. Soc.* **2009**, *131*, 11302.
- (36) Bongiorno, A.; Landman, U. *Phys. Rev. Lett.* **2005**, *95*, 106102.
- (37) Wells, B. A.; Chaffee, A. L. *J. Chem. Phys.* **2008**, *129*, 164712.
- (38) Liu, L. M.; McAllister, B.; Ye, H. Q.; Hu, P. *J. Am. Chem. Soc.* **2006**, *128*, 4017.
- (39) Date, M.; Okumura, M.; Tsubota, S.; Haruta, M. *Angew. Chem., Int. Ed.* **2004**, *43*, 2129.
- (40) Valden, M.; Lai, X.; Goodman, D. W. *Science* **1998**, *281*, 1647.
- (41) Michaelian, K.; Rendon, N.; Garzon, I. L. *Phys. Rev. B* **1999**, *60*, 2000.
- (42) Doye, J. P. K.; Wales, D. J. *New J. Chem.* **1998**, *22*, 733.
- (43) Doye, J. P. K.; Wales, D. J. *J. Chem. Phys. Lett.* **1995**, *247*, 339.
- (44) Delley, B. *J. Chem. Phys.* **1990**, *92*, 508.
- (45) Delley, B. *J. Chem. Phys.* **2000**, *113*, 7756.
- (46) Perdew, J. P.; Wang, Y. *Phys. Rev. B* **1992**, *45*, 13244.
- (47) Ulitsky, A.; Elber, R. J. *J. Chem. Phys.* **1990**, *92*, 1510.
- (48) Grochola, G.; Snook, I. K.; Russo, S. P. *J. Chem. Phys.* **2007**, *127*, 224704.
- (49) Jiang, Q.; Lu, H. M.; Zhao, M. *J. Phys.: Condens. Matter* **2004**, *16*, 521.
- (50) Gajdos, M.; Eichler, A.; Hafner, J. *J. Phys.: Condens. Matter* **2004**, *16*, 1141.
- (51) Termentzidis, K.; Hafner, J. *J. Phys.: Condens. Matter* **2007**, *19*, 246219.
- (52) Lide, D. R., Ed. *CRC Handbook of Chemistry and Physics*, 81st ed.; CRC Press: Boca Raton, FL, 2000.
- (53) Liu, D.; Lian, J. S.; Jiang, Q. *J. Phys. Chem. C* **2009**, *113*, 1168.
- (54) Blyholder, G. *J. Phys. Chem.* **1964**, *68*, 2772.
- (55) Xu, Y.; Getman, R. B.; Shelton, W. A.; Schneider, W. F. *Phys. Chem. Chem. Phys.* **2008**, *10*, 6009.
- (56) Gong, X. Q.; Liu, Z. P.; Raval, R.; Hu, P. *J. Am. Chem. Soc.* **2004**, *126*, 8.
- (57) Alavi, A.; Hu, P. J.; Deutsch, T.; Silvestrelli, P. L.; Hutter, J. *Phys. Rev. Lett.* **1998**, *80*, 3650.

JP107251A